Materials and Design 31 (2010) 2375–2380

Contents lists available at ScienceDirect

Materials and Design

journal homepage: www.elsevier.com/locate/matdes

Microstructure and tensile properties of friction welded aluminum alloy AA7075-T6

H. Khalid Rafi *, G.D. Janaki Ram, G. Phanikumar, K. Prasad Rao

Materials Joining Laboratory, Dept. of Metallurgical and Materials Engineering, Indian Institute of Technology Madras, Chennai 600 036, India

ARTICLE INFO

Article history:
Received 25 September 2009
Accepted 28 November 2009
Available online 3 December 2009

Keywords:
Aluminum alloys
Friction welding
Taguchi method
Microstructure
Tensile properties

ABSTRACT

Solid-state welding processes like friction welding and friction stir welding are now being actively considered for welding aluminum alloy AA7075. In this work, friction welding of AA7075-T6 rods of 13 mm diameter was investigated with an aim to understand the effects of process parameters on weld microstructure and tensile properties. Welds made with various process parameter combinations (incorporating Taguchi methods) were subjected to tensile tests. Microstructural studies and hardness tests were also conducted. The results show that sound joints in AA7075-T6 can be achieved using friction welding, with a joint efficiency of 89% in as-welded condition with careful selection of process parameters. The effects of process parameters are discussed in detail based on microstructural observations.

1. Introduction

Aluminum Alloy AA7075 (Al–Zn–Mg–Cu) is one of the strongest aluminum alloys in industrial use today. Its high strength-to-weight ratio, together with its natural aging characteristics, makes it attractive for a number of aircraft structural applications [1]. The alloy derives its strength from precipitation of Mg_2Zn and Al_2CuMg phases. A major problem with this alloy is that it is not fusion weldable. It is extremely sensitive to weld solidification cracking as well as heat-affected zone (HAZ) liquation cracking due to the presence of copper. While it is possible to overcome the problem of weld solidification cracking using a suitable non-heat-treatable aluminum alloy filler (for example, Al–Mg or Al–Si), the resulting joint efficiencies are unacceptably low [2]. Further, oxidation and/or vaporization of zinc present several problems during welding, such as porosity, lack-of-fusion, and hazardous fumes. Therefore, use of alloy AA7075 is currently limited to applications that do not involve welding [3].

Given these problems in fusion welding, use of solid-state welding processes, like friction welding and friction stir welding, is attractive for alloy AA7075. Because melting and solidification are not involved in these processes, there are no issues with solidification cracking, liquation cracking, segregation, formation of brittle eutectics/intermetallics, etc. Since no filler material is added in these processes, the weld composition is the same as that of the base material. Further, solid-state welding processes typically result in fine-grained wrought microstructures with superior joint mechanical properties compared to the cast fusion weld microstructures. Solid-state welding processes, apart from being environmentally friendly, have several other advantages such as narrow HAZ and low residual stresses and distortion [4,5].

Friction welding is now an established solid-state welding process, with a number of industrial applications realized in aerospace, automobile, defence, and other industries. In this process, parts to be joined are rotated against each other, while applying some axial force (friction force). As they are rotated, the surface oxide layers are broken up and heat generates at the weld interface due to friction, which locally softens the materials. As the parts continue to rotate, more heat generates, and the materials at the weld interface begin to plastically deform. The broken oxide layers are taken away from the weld interface by an outward plastic metal flow (which manifests as flash) and nascent metal surfaces are brought to intimate contact. The parts are then abruptly brought to rest and a higher axial force is applied to complete the weld. Some of the specific advantages of friction welding compared to other solid-state welding processes are: (i) extremely short welding times, (ii) no special tooling, clamping, atmosphere control or surface preparation required, (iii) suitability for welding rod/pipe geometries and for welding dissimilar metal combinations [6,7].

Friction welding of aluminum alloys has been widely reported [8–10], although the information available on alloy AA7075 is scanty. Kimura and co-workers have studied the joining phenomena during friction welding of AA7075-T6. They found that the mechanism of AA7075 friction welding was similar to that of low carbon steel and attributed this to the similarities in their strength properties [5]. In another work, the same investigators, using 16 mm diameter AA7075-T6 rods, reported a joint efficiency of 82% in as-welded condition, 90% in post-weld naturally aged condition (after 730 days), and 95% in post-weld artificially aged

* Corresponding author. Tel.: +91 44 22574760; fax: +91 44 22574752.
E-mail address: khalidrafi@gmail.com (H.K. Rafi).

0261-3069/$ - see front matter © 2009 Elsevier Ltd. All rights reserved.
doi:10.1016/j.matdes.2009.11.065

condition [11]. It may be possible to further improve the joint efficiency by using optimum process parameters. Further, very little information is available on AA7075 friction weld microstructures. In view of the above, the current work is undertaken with an aim to systematically investigate the effects of process parameters on microstructure and tensile properties of AA7075-T6 friction welds and to identify the optimum combination of process parameters for maximizing the joint efficiency in as-welded condition.

2. Experimental work

AA7075 rods (Al–2.44Zn–5.79 Mg–1.66Cu–0.22Fe) of 13 mm diameter were machined out from 15 mm thick rolled plates. The rods are then solution treated (at 480 °C for 2 h) and artificially aged (at 120 °C for 24 h). Fig. 1 shows the microstructure of the base metal rods (corresponding to the longitudinal section of the original plate). A large number of undissolved second-phase particles were seen in the microstructure; these are known to be Al_2Cu_2Fe and/or $Al_{23}CuFe_4$ [12].

Surface preparation is generally not considered a major requirement in friction welding, as the surface irregularities get removed by the scouring action during friction stage and the debris gets removed in flash. However, Yilbas et al. [9] and Hasui and Matsui [13] showed that surface preparation can significantly affect the joint strength. In the current work, the contact surfaces were machined before welding not only to produce smooth, oxide-free surfaces, but also to ensure perpendicularity, which is also important for achieving sound welds.

The main process parameters in friction welding are spindle speed, friction pressure, upset pressure and burn of length. In the current work, a Taguchi L8 orthogonal array was selected for evaluation of the effects of the process parameters. Two levels were considered for each of the four process parameters, based on preliminary welding trials. Interacting influences between process parameters were not assessed. Table 1 lists all the process parameter combinations investigated in the current work. Ultimate tensile strength of the joint was taken as the response parameter. Friction welding experiments as per Table 1 were conducted in a randomized order using a 200 kN capacity fully automatic continuous drive friction welding machine. For each combination of process parameters three replicates were made. Equal overhang lengths were employed on both stationary and rotating sides in all cases.

Tensile tests were conducted on friction welded samples as per ASTM E8 in a 250 kN Schimadzu machine. Cross-sectional samples for microstructural examination were prepared following standard metallographic procedures. Polished specimens were etched using Keller's regent (92 ml H_2O, 5 ml HNO_3, 3 ml HCl and 2 ml HF). Vickers microhardness measurements were made across the weld interface on polished and etched samples employing a load of 100 gf, applied for 15 s.

Table 1
Taguchi L8 experimental matrix.

Sample #	Spindle speed (rpm)	Friction pressure (MPa)	Upset pressure (MPa)	Burn-off length (mm)
S1	1000	38	152	1
S2	1000	38	304	4
S3	1000	114	152	4
S4	1000	114	304	1
S5	2000	38	152	1
S6	2000	38	304	4
S7	2000	114	152	4
S8	2000	114	304	1

3. Results and discussion

3.1. Process parameter optimization

The results of tensile testing on the welds made using various combinations of process parameters are listed in Table 2. For a given process parameter combination, variation in ultimate tensile strength (UTS) was found to be less than 2%. However, significant differences, ranging from 432 MPa to 555 MPa, were observed in UTS among the various welds, indicating that the process parameters have a strong bearing on the quality of joints. Among the eight weld samples, Samples S1 and S7 showed the lowest (432 MPa) and highest (555 MPa) UTS values, respectively. Weld strength, in all cases, was found to be less than that of the base material in T6 condition (623 MPa). All the samples were found to fail in the weld region (Fig. 2).

The aim of this investigation is to evaluate the effects of process parameters on joint strength. Towards this end, Analysis of Variance (ANOVA) was performed using the ultimate tensile strength as the response parameter (the higher the better), following

Table 2
Results of tensile tests.

Ultimate tensile strength (MPa)				
Sample #	Replicate 1	Replicate 2	Replicate 3	Average
S1	435	433	428	432
S2	476	469	468	471
S3	497	497	491	495
S4	455	448	450	451
S5	452	453	457	454
S6	472	477	470	473
S7	558	550	557	555
S8	550	544	547	547

Note: Ultimate tensile strength of the base material in T6 condition: 623 MPa.

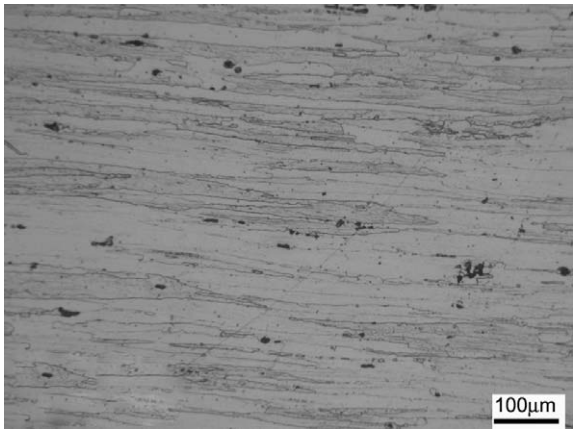

Fig. 1. Microstructure of AA7075 rods in T6 condition.

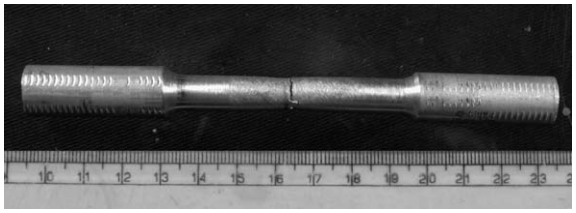

Fig. 2. Fractured weld tensile specimen (Sample S7).

standard ANOVA procedure [14]. Table 3 summarizes the results of ANOVA. As can be seen, friction pressure, spindle speed, and burn-off length have statistically significant influence on joint strength. Among these three, friction pressure was found to have the strongest effect on joint strength followed by spindle speed and burn-off length. On the other hand, the effect of upset pressure, within the parameter range selected in this investigation, was found to be insignificant.

From Table 4, it can be seen that use of higher levels for friction pressure (114 MPa), spindle speed (2000 rpm), and burn-off length (4 mm) is beneficial for maximizing the joint strength. Since upset pressure was found to be statistically insignificant, it can be chosen at the lower level (i.e., 152 MPa), as it helps in minimizing the overall axial reduction and hence, material wastage. This parameter combination (friction pressure: 114 MPa, spindle speed: 2000 rpm, burn-off length: 4 mm, upset pressure: 152 MPa) was the same as the parameter combination used for making Sample S7, which was the one that showed the highest joint strength.

Friction welding is basically a hot deformation process. Intimate contact between nascent surfaces is what is required for achieving sound metallurgical bonding. Plastic deformation plays an important role in facilitating this. The process of friction welding can be divided into three distinct stages: Stages I–III [15]. Early in the friction stage, wear and seizure occur due to the combined effect of coulomb friction and sticking friction. This causes the interface temperature to rise rapidly and, consequently the yield strength of the material decreases [16]. For good joint formation, the temperature rise at the weld interface should be sufficiently high (above 400 °C) so that the flow stress is sufficiently low for ensuring adequate plastic deformation [17]. Friction pressure and spindle speed play an important role in determining the amount of temperature rise at the interface [18,19]. Towards the end of Stage I, a large amount flash results due to plastic metal flow. As this happens, the friction coefficient drop off (as plasticized metal acts as lubricant) and there will be a sudden drop in the rate of heat generation. In Stage II, adiabatic heating due to plastic deformation helps sustain the interface temperature, setting in a dynamic balance between heat generation and heat conduction, while plastic deformation continues to occur at a constant rate under the influence of friction pressure. The extent of Stage II is dependent on the burn-off length. The larger is the burn-off length, the lengthier is Stage II, and the more is the overall heat input to the joint region. In Stage III, the parts are suddenly brought to rest and an upset pressure which is always higher than friction pressure is applied, leading to a large amount of flash and large axial reduction. Sufficient amount of plastic deformation or axial reduction is required in Stage III for achieving sound joints. The extent of axial reduction depends not only on the magnitude of upset pressure but also on the burn-off length, as it influences the duration of Stage II.

The results show that a combination of higher friction pressure, spindle speed, and burn-off-length produces the strongest joint. Higher friction pressure and higher spindle speed ensures high enough temperatures at the weld interface so that adequate plastic deformation occurs during Stages I and II. Use of higher burn-off length helps achieving the minimum plastic deformation required in Stage III. Based on the results obtained in the current work, it appears that as long as a sufficiently high burn-off length is employed, adequate plastic deformation in Stage III can be achieved even with a moderate upset pressure. In fact, Kimura et al. [5] reported a joint efficiency of 82% in AA7075-T6 friction welds, using no forge pressure at all, but compensating for it with a relatively high friction pressure. These observations suggest that upset pressure plays a minor role in friction welding as long as other parameters are appropriately chosen. However, upset pressure could be a deciding factor in realizing good joints in other situations, especially when dealing with dissimilar metals like copper and steel. It should be noted that the optimum parameters reported here are specific to the material and rod diameter used in the current investigation. Further, the results are also machine-specific as certain variables like brake timing, upsetting speed, etc. are machine-dependent, which can considerably influence the outcome of the process.

In the present work, a joint efficiency (tensile strength of weld specimen divided by tensile strength of base metal specimen, expressed in percentage) of 89% in as-welded condition was achieved with optimum process parameter combination, which is considerably higher than in earlier works. It is pertinent to mention that all tensile tests and hardness tests in the current work were conducted on weld samples within a week after welding, which is too short for any significant natural aging to take place. One can expect further improvement in weld strength with time (close to 100% joint efficiency) as alloy AA7075 undergoes natural aging [5,20].

Table 3
ANOVA summary table.

Source	Sum of squares	Degrees of freedom	Variance	F	Percentage contribution
Spindle speed	12,150	1	12,150	87.4	28.5
Friction pressure	17,821	1	17,821	128.2	41.8
Upset pressure	73	1	73	0.52	0.1
Burn-off length	9841	1	9841	70.7	23.1
Error	2654	19	139		6.2

Note: $F_{(\text{table: } 1,19)}$ at 95% confidence = 4.38.

Table 4
Mean response table.

Sample #	Spindle speed (rpm)	Friction pressure (MPa)	Upset pressure (MPa)	Burn-off length (mm)
Level 1	5547	5490	5784	5652
Level 2	6087	6144	5826	5982
Difference	540	654	42	486
Rank	2	1	4	3

3.2. Microstructures

The macrostructures of all the eight different friction welded samples are shown in Fig. 3. As can be seen, welds in all cases are defect-free. The lower tensile strengths values exhibited by Samples S1, S4, and S5 can be related to very little flash formation, which is an indication of inadequate plastic deformation and/or inadequate heat generation. On the other hand, Samples S7 and S8 showed good amount of flash, indicating adequate heat generation, plastic deformation and expulsion of oxide scales and other contaminants. These are consistent with the higher tensile strengths measured on these samples. It should be noted that large flash formation need not always lead to strong joints. For example, Samples S2 and S6 showed very large flash formation compared to all other samples, but the strength values measured on these samples were only moderate. These samples were made using high upset pressure and high burn-off length. This combination leads to excessive deformation in Stage III and, therefore, is undesirable.

Friction welds are known to exhibit three distinct microstructural zones: dynamically recrystallised zone (DRX), thermo-mechanically affected zone (TMAZ), heat-affected zone (HAZ) [8,21,22]. The microstructures of Sample S7 at regions corresponding to mid-radius and center are shown in Fig. 4a and b, respectively, with the three microstructural regions marked on the pictures. The dark central region, DRX, seen in these microstruc-

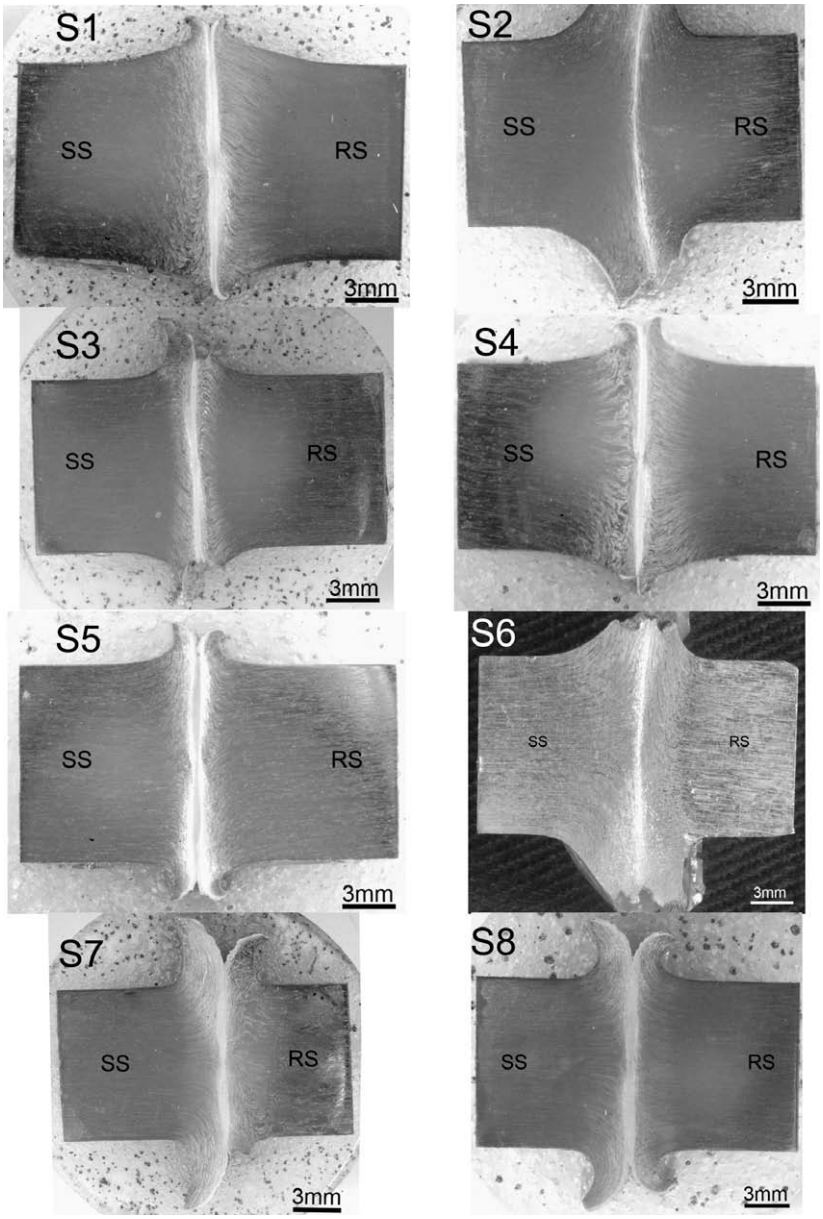

Fig. 3. Macrostructures of friction welds (SS: stationary side, RS: rotating side).

tures (bright vertical lines seen at the interface in the macrostructures presented in Fig. 3) showed extremely fine grains, as can be seen in Fig. 4c. In general, the width of DRX was found to be lower at the center and at the edge of the periphery compared to that at the mid-radius. The lower DRX width at the center is known to be a result of lower linear velocities, whereas the lower DRX width at the periphery is a result of flash formation [11]. Apart from the width of DRX, a distinct region of TMAZ can be noticed at mid-radius which is not quite there at the center, suggesting that the plastic deformation is more at the mid-radius than at the center. Some differences in the width of DRX were seen among the various welds (Fig. 3). It appears that the width of DRX is dependent on how much material is squeezed out in the form of flash during the upsetting stage. For example, Samples S2 and S6 showed thin curved DRX lines, which can be attributed to excessive plastic deformation as a result of high upset pressure and high burn-off length. A comparison of the microstructures of Sample S7 (Fig. 4a) and Sample S2 (Fig. 5) further supports this observation.

Some differences in TMAZ microstructures were also noticed between the stationary and rotating sides of the welds, as can be seen in Fig. 5, for Sample S7 at mid-radius. On the stationary side (Fig. 6a), the grains immediately adjacent to the DRX seem to be oriented almost parallel to the weld interface, indicating smoother plastic metal flow. In contrast, on the rotating side (Fig. 6b), the grain structure did not seem to align well with the weld interface, indicating difficulties in metal flow. This is further evidenced by the fact that the amount of flash formed on the rotating side is always lower than that on the stationary side (Fig. 3). These observations strongly suggest that the thermal and deformation conditions are considerably different on either side of the weld interface. Differences in temperature between the stationary and the rotating sides can arise due to the very fact that former is fixed and the latter is rotating. On the rotating side, high speed rotation can lead to faster heat dissipation due to convection. Since heat dissipation on the stationary side is not as effective as on the rotating side, the stationary side can be expected to experience higher temperatures.

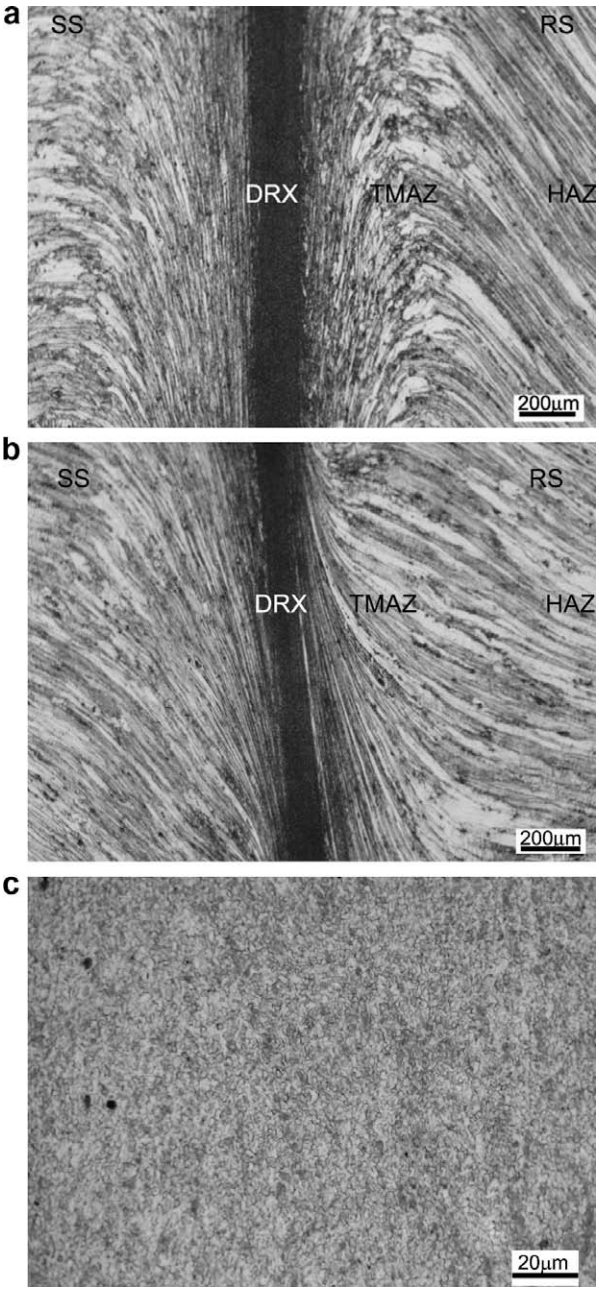

Fig. 4. Microstructures of Sample S7: (a) mid-radius, (b) center, (c) DRX at a higher magnification.

Consequently, more extensive plastic deformation can occur on the stationary side, leading to a larger amount of flash formation. Another difference is that the TMAZ grains on the rotating side (Fig. 6b) very nearer to the DRX, seem to be distinctly finer than those on the stationary side (Fig. 6a). This study gives an understanding about the interfacial microstructural characteristics of AA7075 similar alloy friction welds. However, further studies are required to fully understand the mechanisms responsible for these microstructural differences and their impact on weld properties. These issues assume greater importance in friction welding of dissimilar metals.

Fig. 7 shows the microstructural features at a region approximately 2 mm away from the weld interface (on the stationary side of Sample S7), where a transition from TMAZ to HAZ is evident. The grain structure in the HAZ appeared to be very similar to that in the unaffected base metal.

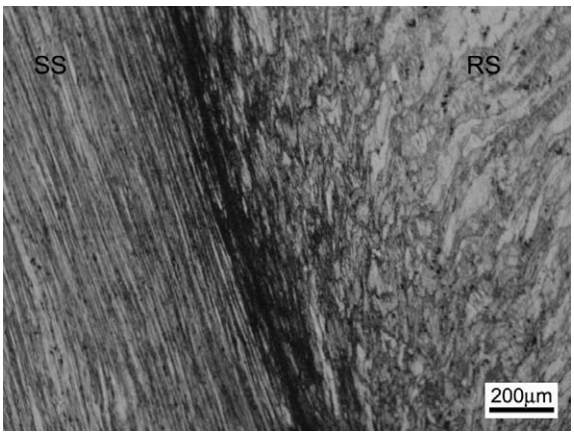

Fig. 5. Narrow DRX in Sample S2 (at mid-radius).

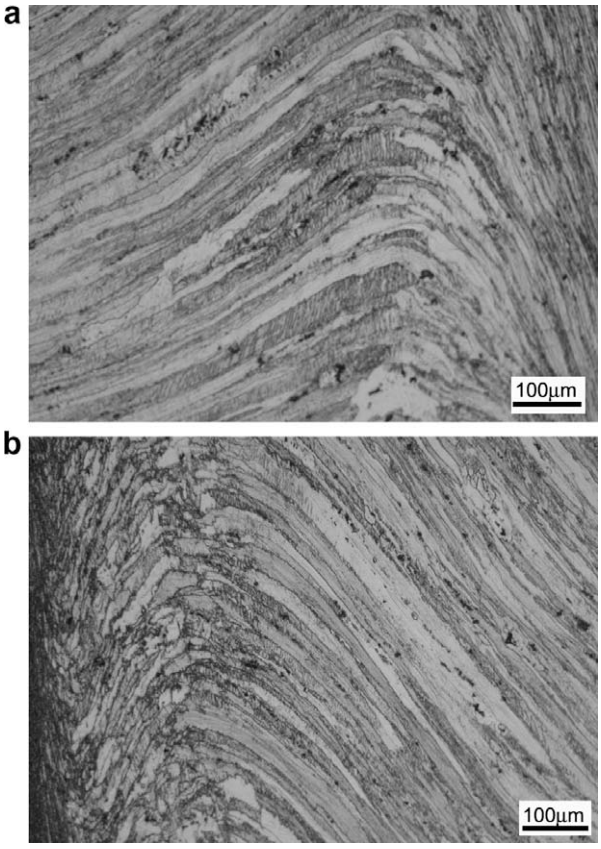

Fig. 6. TMAZ microstructures: (a) stationary side, (b) rotating side.

3.3. Hardness

Vickers microhardness measurements were made across the weld on Sample S7 to see how the process affected strengthening precipitation in the three microstructural zones of the weld. Fig. 8 shows the hardness profile across the weld interface. The hardness profile can be seen to be more or less symmetric about the weld interface. On both stationary and rotating sides, there is a significant drop in hardness in the HAZ and TMAZ regions. On the rotating side, the TMAZ hardness was found to be higher than the HAZ hardness. This was, however, not clearly observed on the stationary side. In the DRX, considerable increase in hardness was observed compared to HAZ.

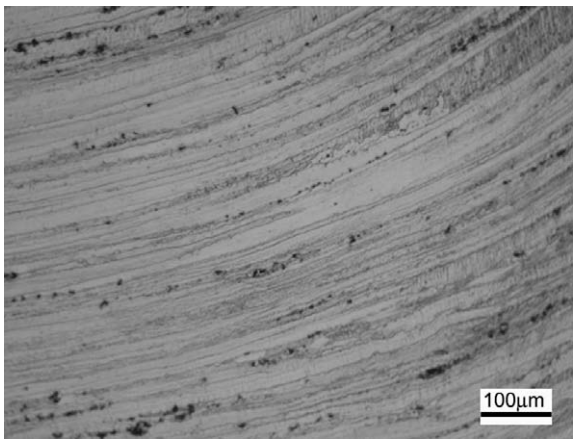

Fig. 7. Transition from TMAZ to HAZ, occurring at approximately 2 mm away from the weld interface (Sample S7).

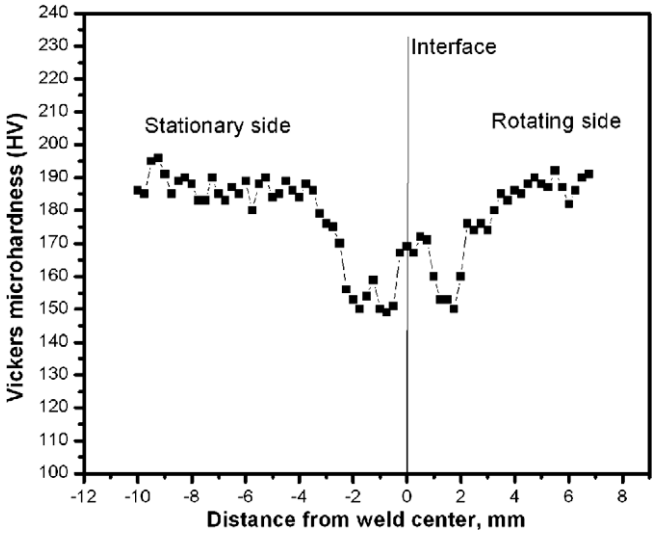

Fig. 8. Hardness profile across the interface.

The drop in HAZ and TMAZ hardness can be explained based on strengthening precipitation. Alloy AA7075 base metal in T6 condition contains a large number of submicroscopic Mg_2Zn and Al_2CuMg precipitate particles, which confer high strength and hardness to the alloy. During friction welding, the HAZ/TMAZ experiences high enough temperatures for causing dissolution or coarsening of these strengthening precipitates. During cooling, the cooling rates are high enough to allow any reprecipitation of these strengthening phases. This explains why HAZ/TMAZ hardness is lower than base metal hardness. The extent of precipitate dissolution or coarsening depends on the peak temperatures and times experienced by the HAZ/TMAZ. Since these can be expected to be different for different combinations of process parameters, weld tensile strength levels can accordingly be different. In the case of DRX, once again, absence of strengthening precipitation by dissolution is what is responsible for its lower hardness when compared to the base metal. The DRX hardness, however, is not as low as the HAZ hardness because of its extremely fine grained microstructure. As already noted, the TMAZ hardness is considerably higher than the HAZ hardness on the rotating side. This can be attributed to the presence of relatively finer grains and/or work hardening effects in the TMAZ microstructure on the rotating side.

4. Conclusions

1. Sound joints in AA7075-T6 can be achieved using friction welding, with a joint efficiency of 89% in as-welded condition with careful selection of process parameters.
2. Friction pressure, spindle speed and burn-off length are the three most significant parameters affecting the joint strength in friction welding of AA7075. Use of higher friction pressure (114 MPa), higher spindle speed (2000 rpm), higher burn-off length (4 mm), and lower upset pressure (152 MPa) are recommended for friction welding of 13 mm diameter rods of AA7075-T6.
3. Welds in all cases showed considerable differences in the amount of flash and in the TMAZ microstructures between stationary and rotating sides. This study brings out characteristics features at the weld interface of AA 7075 similar alloy friction welds, particularly, the influence of stationary sides and rotating sides on micro structural features. Further work is needed to understand the mechanisms responsible for these effects and their impact on weld properties.

References

[1] Abhay K Jha, Sreekumar K. Metallurgical studies on cracked Al–5.5Zn–2.5Mg–1.5Cu aluminum alloy injector disc of turbine rotor. J Fail Anal Preven 2008;8(4):327–32.
[2] Balasubramanian V, Ravisankar V, Madhusudhan Reddy G. Effect of postweld aging treatment on fatigue behavior of pulsed current welded AA7075 aluminum alloy joints. J Materi Eng Perform 2008;7(2):224–33.
[3] Gupta RK, Ramkumar P, Ghosh BR. Investigation of internal cracks in aluminum alloy AA7075 forging. Eng Fail Anal 2006;13:1–8.
[4] Venugopal T, Srinivasa Rao K, Prasad Rao K. Studies on friction stir welded AA7075 aluminum alloy. Trans Indian Inst Met 2004;57(6):659–63.
[5] Kimura M, Kusaka M, Seo K, Fuji A. Joining phenomena during friction stage of AA7075-T6 aluminum alloy friction weld. Sci Technol Weld Join 2005;10(3):378–83.
[6] Maalekian M. Friction welding – critical assessment of literature. Sci Technol Weld Join 2007;12(8):738–59.
[7] Bekir S Yilbas, Ahmet Z Sahin, Nafiz Kahraman, Ahmed Z A1-Garni. Friction welding of St–A1 and A1–Cu materials. J Mater Process Technol 1995;49:431–43.
[8] Lee WB, Yeon YM, Kim DU, Jung SB. Effect of friction welding parameters on mechanical and metallurgical properties of aluminum alloy 5052-A36 steel joint. Mater Sci Technol 2003;19:773–8.
[9] Bekir S Yilbas, Ahmet Z Sahin, Ali Coban, Abdul Aleem BJ. Investigation into the properties of friction-welded aluminium bars. J Mater Process Technol 1995;54:76–81.
[10] Kimura M, Choji M, Kusaka1 M, Seo1 K, Fuji A. Effect of friction welding conditions on mechanical properties of A5052 aluminium alloy friction welded joint. Sci Technol Weld Join 2006;11(2):209–15.
[11] Kimura M, Choji M, Kusaka M, Seo K, Fuji A. Effect of friction welding conditions and aging treatment on mechanical properties of AA7075-T6 aluminum alloy friction joints. Sci Technol Weld Join 2005;10(4):406–12.
[12] Pao PS, Gill SJ, Feng CR. On fatigue crack initiation from corrosion pits in 7075-T7351 aluminum alloy. Scripta Mater 2000;43:391–6.
[13] Atsushi Hasui, Takashi Matsui. On the effect of faying face condition on weldability in friction welding. Trans Jpn Weld Soc 1987;18:77–82.
[14] Ross PJ. Taguchi techniques for quality engineering. New York: McGraw-Hill Book Company; 1988.
[15] Midling OT, Grong O. A process model for friction welding of A1–Mg–Si alloys and A1–SiC metal matrix composites-1. HAZ temperature and strain rate distribution. Acta Metal Mater 1994;42(4):1595–609.
[16] Maalekian M, Kozeschink E, Brantner HP, Cerjak H. Comparative analysis of heat generation in friction welding of steel bars. Acta Mater 2008;56:2843–55.
[17] Zhang H, Lin GY, Peng DS, Yang LB, Lin QQ. Dynamic and softening behaviors of aluminum alloys during multistage hot deformation. J Mater Process Technol 2004;148:245–9.
[18] Kozo Okita, Masatoshi Aritoshi. Measurement of friction temperature under steady state by conventional driving method. Trans Jpn Weld Soc 1982;13(2):9–14.
[19] Andrezej Sluzalec. Thermal effects in friction welding. Int J Mech Sci 1990;32(6):467–78.
[20] Linton VM, Ripley MI. Influence of time on residual stresses in friction stir welds in age hardenable 7xxx aluminum alloys. Acta Mater 2008;56:4319–27.
[21] Lin CB, Chiang Chou, Ma CL. Manufacturing and friction welding properties of particulate reinforced 7005 Al. J Mater Sci 2002;37:4645–52.
[22] Fukumoto S, Tsubakino H, Aritoshi M, Tomita T, Okita K. Dynamic recrystallisation phenomena of commercial purity aluminium during friction welding. Mater Sci Technol 2002;18:219–25.